KINETICS OF THE WIDMANSTÄTTEN FERRITE TRANSFORMATION IN STEEL

S. J. Jones and H. K. D. H. Bhadeshia
Department of Materials Science & Metallurgy,
University of Cambridge, Pembroke St.,
Cambridge, CB2 3QZ, United Kingdom

Abstract

Widmanstätten ferrite grows by a paraequilibrium displacive mechanism but it rarely occurs in isolation in steels. It is usually preceded by the formation of allotriomorphic ferrite by a reconstructive transformation mechanism. In this paper, we deal with a novel modification of the Avrami overall transformation kinetics theory as adapted by Cahn, for grain boundary nucleated phases. Our modification deals with the simultaneous occurrence of two or more transformations. The method is demonstrated to faithfully reproduce published data on the volume fractions of allotriomorphic and Widmanstatten ferrite as a function of chemical composition, austenite grain size and heat treatment (isothermal or continuous cooling transformation).

INTRODUCTION

An understanding of Widmanstätten ferrite is important because it is a phase which greatly influences the mechanical properties of steels. There are many investigations which suggest that Widmanstätten ferrite can be detrimental to toughness [1]. It tends to grow in packets of plates which are in identical crystallographic orientation, allowing cracks to propagate across packets without much deviation.

Watson and McDougall [2] demonstrated that when Widmanstätten ferrite grows, the shape of the transformed region changes. This shape deformation is an invariant–plane strain (IPS) with a large shear component and is a characteristic of displacive transformation. Carbon nevertheless has to partition into the austenite during the growth of Widmanstätten ferrite. The transformation is therefore classified as a paraequilibrium displacive transformation. The growth rate of Widmanstätten ferrite can therefore be calculated using the theory for the carbon–diffusion controlled growth of plate shapes after allowing for an appropriate amount of strain energy due to the IPS shape change [3]. Its nucleation mechanism is also understood to the extent that it is possible to calculate the transformation–start temperature (W_S) and the rate as a function of undercooling below W_S [4,5]. It should therefore be possible to estimate the overall transformation kinetics as a function of the steel composition and heat treatment.

However, Widmanstätten ferrite rarely occurs in isolation. It is usually preceded by the formation of allotriomorphic ferrite at the austenite grain surfaces and there may be other transformations such as pearlite which compete with Widmanstätten ferrite [6]. Therefore, to model the kinetics of the Widmanstätten ferrite transformation (*i.e.* the purpose of this paper), it is necessary to develop theory capable of handling several simultaneous precipitation reactions which can in principle interfere with each other both spatially and in terms of solute partitioning.

The evolution of volume fraction during solid–state transformation can be modelled using the classical Johnson–Mehl–Avrami theory, which has been reviewed by Christian [7]. We introduce this in order to set the scene for the modifications made to allow for simultaneous reactions.

OVERALL TRANSFORMATION KINETICS

A given precipitate particle effectively forms after an incubation period τ. Assuming growth at a constant rate G, the volume w_τ of a spherical particle is given by

$$w_\tau = (4\pi/3)G^3(t-\tau)^3 \qquad (t > \tau) \qquad (1)$$

with $w_\tau = 0$ for $(t < \tau)$ where t is the time defined from instant the sample reaches the isothermal transformation temperature.

Displacive Phase Transformations and Their Applications in Materials Engineering
Edited by K. Inoue, K. Mukherjee, K. Otsuka, and H. Chen
The Minerals, Metals & Materials Society, 1998

Particles nucleated at different locations may eventually touch; this problem of hard impingement is neglected at first, by allowing particles to grow through each other and by permitting nucleation to happen even in regions which have already transformed. The calculated volume of β phase is therefore an *extended volume*. The change in extended volume due to particles nucleated in a time interval $t = \tau$ to $t = \tau + d\tau$ is, therefore,

$$dV_\beta^e = w_\tau I V d\tau$$
$$V_\beta^e = (4\pi V/3)\int_{\tau=0}^{t} G^3 I (t-\tau)^3 d\tau \qquad (2)$$

where I is the nucleation rate per unit volume and V is the total sample volume.

Only those parts of the change in extended volume which lie in untransformed regions of the parent phase can contribute to the change in real volume of β. The probability that any change in extended volume lies in untransformed parent phase is proportional to the fraction of untransformed material. It follows that the actual change in volume in the time interval t to $t+dt$ is

$$dV_\beta = \left(1 - \frac{V_\beta}{V}\right) dV_\beta^e$$
$$V_\beta^e = -V \ln\left(1 - \frac{V_\beta}{V}\right)$$

so that

$$-\ln\left(1 - \frac{V_\beta}{V}\right) = (4\pi/3)G^3 \int_0^t I(t-\tau)^3 d\tau \qquad (3)$$

This approach is limited to the precipitation of a single phase; it can be applied to cases where more than one decomposition reaction occurs, if the individual reactions occur over different temperature ranges, *i.e.* they occur successively and largely independently [8,9]. This is not the case in practice. The adaptation of the Johnson–Mehl–Avrami approach to deal with many reactions occurring simultaneously is illustrated with a simple example below.

SIMULTANEOUS REACTIONS

The principles involved are first illustrated with a simplified example in which α and β precipitate at the same time from the parent phase which is designated γ. It is assumed that the nucleation and growth rates do not change with time and that the particles grow isotropically.

The increase in the extended volume due to particles nucleated in a time interval $t = \tau$ to $t = \tau + d\tau$ is, therefore, given by

$$dV_\alpha^e = \frac{4}{3}\pi G_\alpha^3 (t-\tau)^3 I_\alpha V \; d\tau \qquad (4)$$

$$dV_\beta^e = \frac{4}{3}\pi G_\beta^3 (t-\tau)^3 I_\beta V \; d\tau \qquad (5)$$

where G_α, G_β, I_α and I_β are the growth and nucleation rates of α and β respectively, all of which are assumed here to be independent of time. V is the total volume of the system. For each phase, the increase in extended volume will consist of three separate parts. Thus, for α:

(a) α which forms in untransformed γ.

(b) α which forms in existing α.

(c) α which forms in existing β.

Only α formed in untransformed γ will contribute to the real volume of α. On average a fraction $[1-(V_\alpha + V_\beta)/V)]$ of the extended volume will be in previously untransformed material. It follows that the increase in real volume of α in the time interval t to $t+dt$ is given by

$$dV_\alpha = \left(1 - \frac{V_\alpha + V_\beta}{V}\right) dV_\alpha^e$$

and similarly for β,

$$dV_\beta = \left(1 - \frac{V_\alpha + V_\beta}{V}\right) dV_\beta^e$$

In general, V_α will be some complex function of V_β and it is not possible to integrate these expressions to find the relationship between the real and extended volumes. However, in certain simple cases it is possible to relate V_α to V_β by multiplication with a suitable constant, K, in which case $V_\beta = KV_\alpha$

The equations relating the increment in the real volume to that of the extended volume can therefore be written as

$$dV_\alpha = \left(1 - \frac{V_\alpha + KV_\alpha}{V}\right) dV_\alpha^e \qquad (6)$$

$$dV_\beta = \left(1 - \frac{V_\beta + KV_\beta}{KV}\right) dV_\beta^e \qquad (7)$$

They may then be integrated to find an analytical solution relating the extended and real volumes analogous to that for single phase precipitation.

$$\frac{V_\alpha^e}{V} = \frac{-1}{1+K} \ln\left[1 - \frac{V_\alpha}{V}(1+K)\right]$$
$$\frac{V_\beta^e}{V} = \frac{-K}{1+K} \ln\left[1 - \frac{V_\beta}{V}\left(\frac{1+K}{K}\right)\right]$$

The total extended volume fraction is found for each phase by integrating equations 4 and 5 with respect to τ. This gives:

$$\zeta_\alpha = \left(\frac{1}{1+K}\right)\left(1 - \exp\left[-\frac{1}{3}(1+K)\pi G_\alpha^3 I_\alpha t^4\right]\right)$$

$$\zeta_\beta = \left(\frac{K}{1+K}\right)\left(1 - \exp\left[-\frac{1}{3}\left(\frac{1+K}{K}\right)\pi G_\beta^3 I_\beta t^4\right]\right)$$

These equations resemble the well known Avrami equation for single phase precipitation with extra factors to account for the presence of a second precipitate phase. When the volume fraction of both precipitating phases is very small the equations approximate to the expressions for each phase precipitating alone. This is because nearly all of the extended volume then lies in previously untransformed material and contributes to the real volume. As transformation proceeds, the volume fraction of each phase predicted for the phases precipitating simultaneously becomes less than that predicted if the phases were precipitating alone. This is expected, since additional phases reduce the fraction of the extended volume which lies in previously untransformed material.

Since the nucleation and growth rates were assumed to be constant, it is possible to calculate explicitly the value of K, which is given by

$$K = V_\beta / V_\alpha = (I_\beta G_\beta^3)/(I_\alpha G_\alpha^3)$$

An example calculation for the case of linear (*i.e.* constant) growth is presented in Fig. 1, for the case where the growth rate of β is set to be twice that of α (with identical nucleation rates). The final volume fraction of the β phase is eight times that of the α phase because volume fraction is a function of the growth rate cubed.

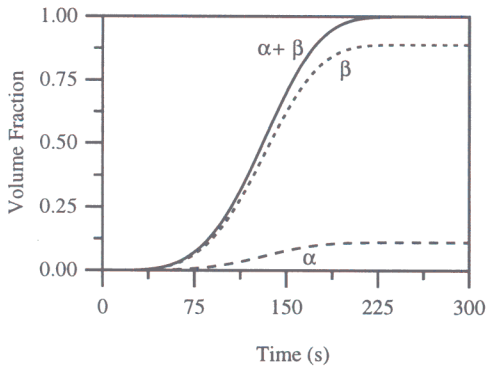

Fig. 1 : Simultaneous precipitation of β and the α. Identical nucleation rates but with β particles growing at twice the rate of the α particles.

COMPLEX SIMULTANEOUS REACTIONS

The analytical expressions discussed above for simultaneous reactions rely on the assumptions of constant nucleation and growth rates, and on a random distribution of nucleation sites. None of these are relevant for the present purposes. For the phases of interest (allotriomorphic and Widmanstätten ferrite, and pearlite) the nucleation and growth rates change with the progress of the transformation as the composition of the austenite changes and the nucleation sites are grain surfaces.

There are two applications of the Avrami extended space idea for grain boundary nucleated reactions, the first applying to the gradual elimination of free grain boundary area and the second to the gradual elimination of volume of untransformed material [10]. If we consider a particular boundary of area O_b, for a system with n phases, we have for the j'th phase,

$$dO_j = \left(1 - \frac{\Sigma_{i=1}^n O_i}{O_b}\right) dO_j^e \qquad (8)$$

where dO_j is the change in the area intersected by phase j on a plane parallel to the boundary but at a distance y normal to that boundary, during the small time interval t to $t+\Delta t$. dO_j^e is similarly, the change in *extended* area of intersection with the same plane at y. This may have a contribution from particles nucleated throughout the period $t = 0$ to $t = m\Delta t$, where m is an integer, so that

$$dO_j^e = O_b \Sigma_{k=0}^m (I_{j,k}\Delta\tau)(A_{j,k,y}\Delta t)$$

where $A_{j,k,y}$ is the rate of change of area of intersection on plane y of a particle which nucleated at $\tau = k\Delta\tau$. The number of such extended particles is $(O_b I_{j,k}\Delta\tau)$ where I is the nucleation rate per unit area.

To obtain a change in the extended volume of the phase j it is necessary to integrate as follows:

$$dV_j^e = \int_{y=0}^{q_j^{max}} dO_j dy$$

where q_j^{max} is the maximum size of a particle of phase j in a direction normal to the grain boundary plane. It follows that the change in real volume is

$$dV_j = \left(1 - \frac{\Sigma_{i=1}^n V_i}{V}\right) dV_j^e \qquad (9)$$

This instantaneous value of dV_j, together with corresponding changes in the volumes of the other $n-1$ phases, can be used to update the total volume of each phase in a computer implemented numerical procedure by writing

$$V_{j,t+\Delta t} = V_{j,t} + dV_{j,t} \qquad \text{for} \qquad j = 1 \ldots n$$

so that a plot of the fraction of each phase can be obtained as a function of time. The growth and nucleation rates can also be updated during this step,

should they have changed because of solute enrichment in the matrix or because there is a change in temperature during continuous cooling transformation.

The next section explains how these equations apply for the allotriomorphic ferrite, Widmanstätten ferrite and pearlite.

ALLOTRIOMORPHIC FERRITE

Classical nucleation theory is used to model the nucleation of allotriomorphic ferrite, with the grain boundary nucleation rate per unit area given by:

$$I = C_1 \frac{kT}{h} \exp\{-\frac{G^* + Q}{RT}\} \exp\{-\frac{\tau_*}{t}\} \qquad (10)$$

where h is the Planck constant, k is the Boltzmann constant, $C_1 = 1.214 \times 10^{12}\,\mathrm{m}^{-2}$ is a fitted constant [11], R is the universal gas constant and $Q = 200\,\mathrm{kJ\,mol}^{-1}$ is a constant activation energy representing the barrier to the transfer of atoms across the interface. The activation energy for nucleation, $G^* = C_2\sigma^3/\Delta G^2$, where σ represents the interfacial energy per unit area, $C_2 = 5.58$ and $\sigma = 0.022\,\mathrm{J\,m}^{-2}$, another fitted constant and ΔG is the maximum chemical free energy change per unit volume available for nucleation [12]. The second exponential relates to the achievement of a steady–state nucleation rate; $\tau_* = n_c^2 h(4a_c kT)^{-1} \exp\{Q/RT\}$, where n_c is the number of atoms in the critical nucleus and a_c is the number of atoms of the critical nucleus which are at the interface [7].

The growth of allotriomorphic ferrite is assumed to occur under paraequilibrium conditions, so that the half–thickness q of the layer during isothermal growth is given by:

$$q = \alpha_1 (t - \tau)^{1/2} \qquad (11)$$

where α_1 is the one–dimensional parabolic thickening rate constant. The growth rate slows down as the particle grows the concentration gradient ahead of the moving interface decreases to accommodate the solute that is partitioned into the austenite. The growth along the grain boundary is taken to be three times that normal to it, giving an aspect ratio of three [13].

The parabolic rate constant is obtained by solving the equation [7]:

$$2\left(\frac{\underline{D}}{\pi}\right)^{\frac{1}{2}} f_1 = \alpha_1 \exp\{\frac{\alpha_1^2}{4\underline{D}}\} \mathrm{erfc}\{\frac{\alpha_1}{2\underline{D}^{\frac{1}{2}}}\}$$

$$\text{with} \qquad f_1 = \frac{x^{\gamma\alpha} - \overline{x}}{x^{\gamma\alpha} - x^{\alpha\gamma}}$$

and where $x^{\gamma\alpha}$ and $x^{\alpha\gamma}$ are the paraequilibrium carbon concentrations in austenite and ferrite respectively at the interface (obtained using a calculated multicomponent phase diagram), $\overline{x}$ is the average carbon concentration in the alloy and $\underline{D}$ is a weighted average diffusivity [14] of carbon in austenite, given by:

$$\underline{D} = \int_{x^{\gamma\alpha}}^{\overline{x}} \frac{D\{x\}\, dx}{\overline{x} - x^{\gamma\alpha}}$$

where D is the diffusivity of carbon in austenite at a particular concentration of carbon.

WIDMANSTÄTTEN FERRITE

There is fine detail in TTT (time–temperature–transformation) diagrams, but they consist essentially of two C–curves (Fig. 2). One of these represents reconstructive transformations at elevated temperatures where atoms are mobile within the time scale of the usual experiments on steels. The lower temperature C–curve represents displacive transformations such as Widmanstätten ferrite and bainite.

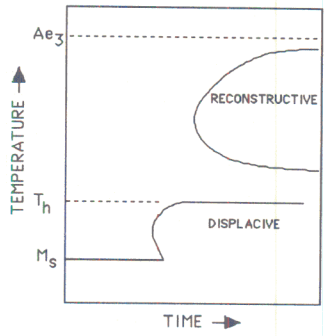

Fig. 2: Schematic TTT diagram illustrating the two C–curves and the T_h temperature.

The lower C–curve has a flat top; the temperature corresponding to this flat top is identified as T_h, the highest temperature at which displacive transformation occurs during isothermal heat–treatment. T_h is either the Widmanstätten ferrite–start (W_S) or bainite–start (B_S) temperature depending on the driving force available at T_h for the steel concerned.

Fig. 3 shows two plots; the first is a calculation of the driving force for the paraequilibrium nucleation of ferrite at T_h, allowing carbon to partition between the austenite and ferrite. The second is the case where there is no partitioning at all during the nucleation of ferrite.

It is evident that the nucleation of Widmanstätten ferrite or bainite cannot in general occur without the partitioning of carbon. The second interesting point is that the curve illustrated in Fig. 3a is linear. This

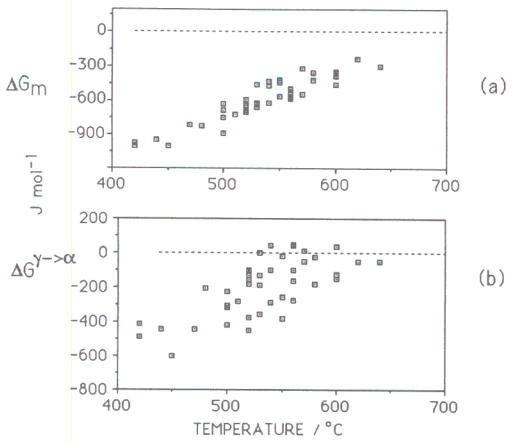

Fig. 3: Curves representing the free energy change necessary in order to obtain a detectable degree of transformation to Widmanstätten ferrite or bainite. Note that each point represents a different steel. (a) The free energy change assuming paraequilibrium nucleation. (b) The free energy change assuming partitionless nucleation.

straight line, which represents all steels, is henceforth called the *universal G_N function* and is given by:

$$G_N = 3.637(T - 273.18) - 2540 \qquad \mathrm{J\,mol^{-1}} \quad (12)$$

with G_N giving the minimum free energy change necessary to nucleate Widmanstätten ferrite or bainite in any steel.

A linear relation such as this cannot be explained by nucleation based on heterophase fluctuations. Consider a nucleation rate (I_V) equation:

$$I_V \propto \nu \exp -G^*/kT \quad (13)$$

where ν is an attempt frequency and all the other terms have their usual meanings. When this is rearranged, we get

$$-G^* \propto \beta T \quad (14)$$

where $\beta = kT \ln\{I_V/\nu\}$. Consequently, the G_N versus T relation can only be linear if

$$G^* \propto G_N \quad (15)$$

and not the inverse square relationship implied by classical nucleation theory. This is entirely consistent with the theory for martensitic nucleation [15].

What then are the conditions which determine whether at T_h, it is Widmanstätten ferrite that forms first or bainite?

In order for a phase to form, it must nucleate and grow. Nucleation will occur at T_h when the driving force for nucleation becomes less than G_N:

$$\Delta G \leq G_N \quad (16)$$

The nucleated phase can develop into Widmanstätten ferrite if a further condition is satisfied, that the driving force for paraequilibrium growth exceeds the stored energy of Widmanstätten ferrite, which amounts to about 50 $\mathrm{J\,mol^{-1}}$.

For the theory presented here, the nucleation rate per unit area is given by

$$I = \frac{1}{2C_3} \exp\left\{-\frac{C_4}{RT} - \frac{C_4 \Delta G}{C_5 RT}\right\} \quad (17)$$

where $C_3 = 6.78\times10^{-10}\,\mathrm{m^2 s}$, $C_4 = 2.065\times10^4\,\mathrm{J\,mol^{-1}}$ and $C_5 = 2540\,\mathrm{J\,mol^{-1}}$, all of which are constants determined by fitting to experimental data [11]. The equation applies below the Widmanstätten ferrite start temperature.

Trivedi has given a solution for the problem of the diffusion-controlled growth of plates. The shape of the plates is taken to be that of a parabolic cylinder and is assumed to be constant throughout growth. The plate lengthening rate (V_l) at a temperature T for steady state growth is obtained by solving the equation:

$$\begin{aligned} f_1 =& (\pi p)^{0.5} \exp\{p\} \mathrm{erfc}\{p^{0.5}\} \\ & [1 + (r_c/r) f_1 S_2\{p\}] \end{aligned} \quad (18)$$

where the Péclet number p, which is a dimensionless velocity, is given by $p = V_l r/2\underline{D}$ The weighted-average diffusion coefficient for carbon in austenite is used as before, but with the integral evaluated over the range $\overline{x}$ to x_r, where x_r is the carbon concentration in the austenite at the plate tip. x_r may significantly differ from the equilibrium carbon concentration $x^{\gamma\alpha}$ because of the Gibbs-Thompson capillarity effect [7] which allows for the change in equilibrium concentration as a function of interface curvature; x_r decreases as interface curvature increases, and growth ceases at a critical plate tip radius r_c when $x_r = \overline{x}$. For a finite plate tip radius(r),

$$x_r = x^{\gamma\alpha}[1 + (\Gamma/r)] \quad (19)$$

where Γ is the capillarity constant [7] given by

$$\Gamma = \frac{\sigma V_m}{RT} \frac{(1 - x^{\gamma\alpha})/(x^{\alpha\gamma} - x^{\gamma\alpha})}{1 + [d(\ln \Gamma_1)/d(\ln x^{\gamma\alpha})]} \quad (20)$$

where σ is the interface energy per unit area, taken to be 0.2 $\mathrm{J\,m^{-2}}$, Γ_1 is activity coefficient of carbon in

austenite, and V_m = molar volume of ferrite. Note that for Widmanstätten ferrite, the paraequilibrium concentrations (*e.g.* $x^{\gamma\alpha}$) are calculated after allowing for the 50 J mol^{-1} of stored energy [4].

This assumes that the α composition is unaffected by capillarity, since $x^{\alpha\gamma}$ is always very small. r_c can be obtained by setting $x_r = \overline{x}$. The function $S_2\{p\}$ depends on the Péclet number; it corrects for variation in composition due to changing curvature along the interface and has been numerically evaluated by Trivedi [7]. Consistent with experimental data, we have also assumed the Zener hypothesis that the plate tip adopts a radius which is consistent with the maximum rate of growth [3,7].

PEARLITE

The nucleation of pearlite is treated as for allotriomorphic ferrite but with a nucleation rate which is two orders of magnitude smaller. This is achieved by reducing the number density of nucleation sites.

The growth of pearlite was approximated to occur by a paraequilibrium mechanism, although it never in practice grows in this way. It is also assumed that the majority of diffusion occurs in the austenite just ahead of the transformation front. In these circumstances, the growth rate is given by [16]

$$v_V = \frac{D}{g}\frac{s^2}{s_\alpha s_\theta}\frac{x^{\gamma\alpha} - x^{\gamma\theta}}{x^{\theta\gamma} - x^{\alpha\gamma}}\frac{1}{s}[1 - \frac{s_C}{s}] \qquad (21)$$

where θ represents cementite, α the ferrite within the pearlite and γ the austenite. g is a geometric factor equal to 0.72 in plain carbon steels, s is the interlamellar spacing, whose critical value at which growth stops is s_C and s_α, s_θ are the respective thickness of ferrite and cementite lamellar. The values of s and s_C are estimated empirically [17] and it is assumed that s adopts a value consistent with the maximum rate of growth.

RESULTS AND DISCUSSION

There have been many studies about the occurrence of Widmanstätten ferrite in steels as a function of the chemical composition, austenite grain size and the cooling rate during continuous cooling transformation [*e.g.* 6,18–20]. It is consequently well–established that Widmanstätten ferrite is favoured in austenite with a large grain structure. This is probably because Widmanstätten ferrite is rarely found in isolation but often forms as secondary plates growing from allotriomorphic ferrite layers. The prior formation of allotriomorphic ferrite, which is favoured by a *small* grain size, enriches the residual austenite with carbon, so it is not surprising that a small austenite grain size suppresses Widmanstätten ferrite. For the same reason, the an increase in cooling rate will tend to favour the formation of Widmanstätten ferrite.

These and other concepts are implicitly built into the model presented here. This is because allotriomorphic ferrite, Widmanstätten ferrite and pearlite are allowed to grow together assuming that thermodynamic and kinetic conditions are satisfied. Their interactions are all taken into account during the course of transformation. It follows that it should be possible to reproduce the excellent quantitative data recently published by Bodnar and Hansen [6]. The present analysis is restricted to Fe–Si–Mn–C steel rather than the microalloyed steels also studied by Bodnar and Hansen.

The chemical composition of the steel is given in Table 1. They used heat–treatments which led to three different austenite grain sizes of 30, 55 and 100 μm. In addition, samples were cooled at five different rates; 11, 16, 30, 59 and 100 °C min^{-1}.

Widmanstätten ferrite can nucleate directly from the austenite grain surfaces or indirectly from allotriomorphic ferrite–austenite interfaces. The present model includes both of these scenarios because of an approximation made in the formulation of extended area in equation 8. It is strictly not possible to separate out the contributions dO_j^e from each phase (for all values of y) when the phases grow at different rates. The result of the approximation is therefore to allow Widmanstätten ferrite to form even if the entire austenite grain surface is decorated with allotriomorphic ferrite. This amounts approximately to the case for secondary Widmanstätten ferrite.

C	Si	Mn	Cu	V
0.18	**0.18**	**1.15**	0.09	< 0.003
P	S	Nb	Al	N
0.015	0.030	< 0.005	0.026	0.0073

Table 1: Chemical composition / wt%

The reasonable overall level of agreement between experiment and theory is illustrate in Fig. 4, for all of the data from [6]. In all cases where the allotriomorphic ferrite content is underestimated, the Widmanstätten ferrite content is overestimated. This is expected both because the composition of the austenite changes when allotriomorphic ferrite forms and because its formation changes the amount of austenite that is free to transform to Widmanstätten ferrite.

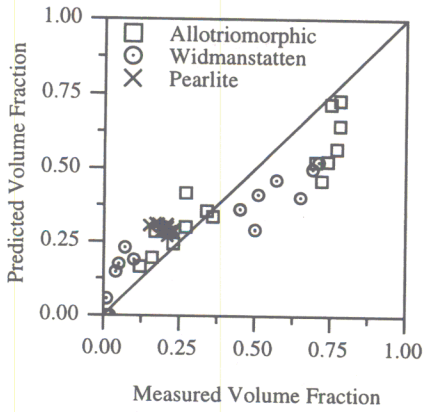

Fig. 4: A comparison of the calculated volume fraction versus experimental data reported by Bodnar and Hansen

MICROSTRUCTURE MAPS

Figures 5–8 show calculations which illustrate how the model can be used to study the evolution of microstructure as the sample cools. The calculations are for the steel composition stated in Table 1.

All of the generally recognised trends are reproduced. The amount of Widmanstätten ferrite clearly increases with the austenite grain size, and with the cooling rate within the range considered. Bodnar and Hansen [6] suggested also that the effect of cooling rate on the amount of Widmanstätten ferrite was smaller than that of the austenite grain size (for the values considered). This is also evident in Figures 5–8.

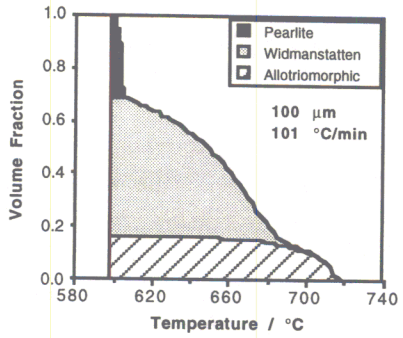

Fig. 5 : Calculated evolution of microstructure in a sample with an austenite grain size of 100 μm, at a cooling rate of 101 °C min^{-1}

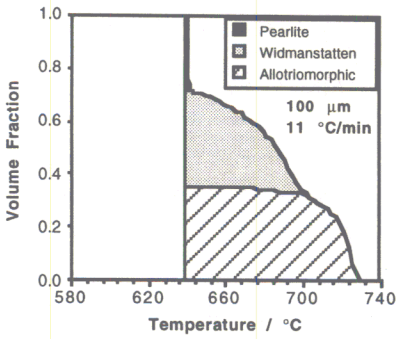

Fig. 6 : Calculated evolution of microstructure in a sample with an austenite grain size of 100 μm, at a cooling rate of 11 °C min^{-1}

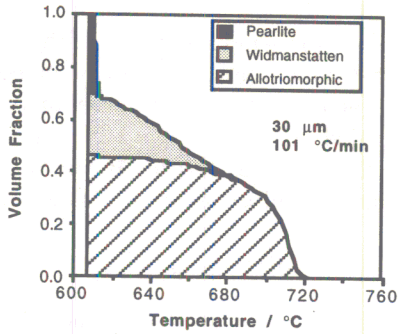

Fig. 7 : Calculated evolution of microstructure in a sample with an austenite grain size of 30 μm, at a cooling rate of 101 °C min^{-1}

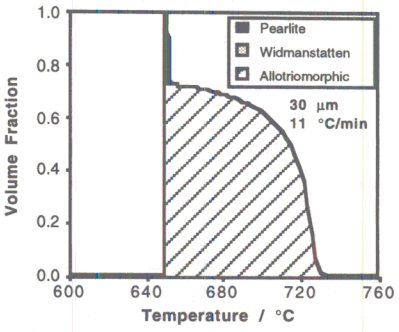

Fig. 8 : Calculated evolution of microstructure in a sample with an austenite grain size of 30 μm, at a cooling rate of 11 °C min^{-1}

SUMMARY

The classical Johnson–Mehl–Avrami theory for overall transformation kinetics has been adapted to deal with the simultaneous formation of allotriomorphic ferrite, Widmanstätten ferrite and pearlite. A comparison with published experimental data has shown that the model developed is reasonable both quantitatively and with respect to well–established trends. The model can now be used to study theoretically, the evolution of microstructure as a function of the alloy composition, the austenite grain size and the cooling conditions. Further work is need to include other phases such as bainite and martensite, and to deal with microalloying additions. It would also be interesting to incorporate nucleation sites other than austenite grain surfaces.

Acknowledgments

We are grateful to the Engineering and Physical Sciences Research Council, and British Steel plc. for supporting this work. It is a pleasure to acknowledge some very helpful discussions with Dr Graham Thewlis. HKDHB is grateful to the Royal Society for a Leverhulme Trust Senior Research Fellowship.

References

1. H. K. D. H. Bhadeshia, "Modelling the elementary mechanical properties of steel welds". *Mathematical Modelling of Weld Phenomena III*, eds. H. Cerjak, B. Buchmayer and H. K. D. H. Bhadeshia, Institute of Materials, London, (1996) 1–50.

2. J. D. Watson and P. G. McDougall, "Crystallography of Widmanstätten ferrite", *Acta Metallurgica* 21 (1973) 961–973.

3. H. K. D. H. Bhadeshia, "Diffusion–controlled growth of ferrite plates in plain carbon steels", *Materials Science and Technology* 1 (1985) 497–504.

4. H. K. D. H. Bhadeshia, "Rationalisation of shear transformations in steels", *Acta Metallurgica* 29 (1981) 1117–1130.

5. G. I. Rees and H. K. D. H. Bhadeshia, "Bainite transformation kinetics", *Materials Science and Technology* 8 (1992) 985–996.

6. R. L. Bodnar and S. S. Hansen, "Effects of Widmanstätten ferrite on the mechanical properties of steel", *Metallurgical and Materials Transactions A* 25A (1994) 763–773.

7. J. W. Christian, *Theory of Transformations in Metals and Alloys,* Part I, 2nd edition, Pergamon Press, Oxford, (1975).

8. M. Umemoto, A. Hiramatsu, A. Moriya, T. Watanabe, S. Nanba, N. Nakajima, G. Anan and Y. Higo, "Computer modelling of phase transformation from deformed austenite", *ISIJ International*, 32 (1992) 306–315.

9. H. K. D. H. Bhadeshia, L.–E. Svensson and B. Gretoft, "Model for the development of microstructure in a low–alloy steel weld deposit", *Acta Metallurgica*, 33 (1985) 1271–1283.

10. J. W. Cahn, "The kinetics of grain boundary nucleated reactions", *Grain boundary nucleated reactions*, 4 (1956) 449-459.

11. S. Jones and H. K. D. H. Bhadeshia, unpublished research, University of Cambridge, 1996.

12. M. Hillert, "The uses of Gibbs free energy–composition diagrams", *Lectures in The Theory of Phase Transformations,* ed. H. I. Aaronson, (1975) 1–50.

13. J. R. Bradley and H. I. Aaronson, "The stereology of grain boundary allotriomorphs", *Metallurgical Trans. A,* 8A (1977) 317–322.

14. R. Trivedi and G. R. Pound, "Effect of concentration dependent diffusion coefficient on the migration of interphase boundaries", *Journal of Applied Physics,* 38 (1967) 3569–3576.

15. G. B. Olson and M. Cohen, "A general mechanism of martensitic nucleation", *Metallurgical Transactions A*, 7A 1897–1923.

16. M. Hillert, "Role of interfacial energy during solid state phase transformations", *Jernkontorets Ann.,* 141 (1957) 757–789.

17. M. Takahashi, "Reaustenitisation from bainite in steels", *Ph.D. Thesis,* University of Cambridge, (1992).

18. R. F. Mehl, C. S. Barrett and D. W. Smith, "Studies upon the Widmanstätten structure, IV, the Fe–C alloys", *Trans. AIMME,* Iron and Steel Division, 105 (1933) 215–258.

19. H. I. Aaronson, D. Eylon, C. M. Cooke, M. Enomoto and F. H. Froes, "The W_S temperature as affected by matrix grain size", *Scripta Metall.,* 23 (1989) 435–440.

20. P. R. Krahe, K. R. Kinsman and H. I. Aaronson, "Influence of austenite grain size on the W_S temperature for the proeutectoid ferrite reaction", *Acta Metallurgica,* 20 (1972) 1109–1121.